Electronic Supplementary Material (ESI) for Dalton Transactions.

Electronic Supplementary Information

Lanthanide salen-type complexes exhibiting single ion magnet and photoluminescent properties

Min Ren, Zhong-Li Xu, Song-Song Bao, Ting-Ting Wang, Ze-Hua Zheng, Rute A. S. Ferreira, Li-Min Zheng* and Luis D. Carlos*

The ac magnetic susceptibilities fitting

The ac magnetic susceptibilities can be well fitted using the generalized Debye model in Eq(S1), Eq(S2)[1]:

$$\chi'(\omega) = \chi_S + \frac{(\chi_T - \chi_S)\left[1 + (\omega\tau)^{1-\alpha}\sin(\pi\alpha/2)\right]}{1 + 2(\omega\tau)^{1-\alpha}\sin(\pi\alpha/2) + (\omega\tau)^{2(1-\alpha)}} \quad \text{(S1)}$$

$$\chi''(\omega) = \frac{(\chi_T - \chi_S)\left[(\omega\tau)^{1-\alpha}\cos(\pi\alpha/2)\right]}{1 + 2(\omega\tau)^{1-\alpha}\sin(\pi\alpha/2) + (\omega\tau)^{2(1-\alpha)}} \quad \text{(S2)}$$

where χ_S is the adiabatic susceptibility, χ_T is the isothermal susceptibility, and τ is the average relaxation time of magnetization, and the α parameter, which ranges between 0 and 1, quantifies the width of the τ distribution.

Calculation of the $^5D_0$ radiative (A_r) and nonradiative (A_{nr}) transition probabilities and quantum efficiency (η)

Based on the emission spectra, the $^5D_0$ A_r and A_{nr} transition probabilities and the quantum efficiency (η)[2-5] was determined for **1** at 300 K. Assuming that only non-radiative and radiative processes are involved in the depopulation of the $^5D_0$ state, η is given by:

$$\eta = \frac{A_r}{A_r + A_{nr}} \quad \text{(S3)}$$

The radiative contribution is calculated from the relative intensities of the $^5D_0 \rightarrow {}^7F_{0\text{-}6}$ transitions. The emission intensity, *I*, taken as the integrated intensity *S* of the emission lines for the $^5D_0 \rightarrow {}^7F_{0\text{-}6}$ transitions, is given by:

$$I_{i\rightarrow j} = \hbar w_{i\rightarrow j} A_{i\rightarrow j} N_i \equiv S_{i\rightarrow j} \quad \text{(S4)}$$

where *i* and *j* represent the initial ($^5D_0$) and final ($^7F_{0\text{-}6}$) levels, respectively, $\hbar\varpi_{i\rightarrow j}$ is the transition energy, $A_{i\rightarrow j}$ the Einstein coefficient of spontaneous emission and N_i the population of the $^5D_0$ emitting level.[3-5] Because the $^5D_0 \rightarrow {}^7F_{5,6}$ transitions are not observed experimentally, their influence on the depopulation of the $^5D_0$ excited state may be neglected and, thus, the radiative contribution is estimated based only on the relative intensities of the $^5D_0 \rightarrow {}^7F_{0\text{-}4}$ transitions. The emission integrated intensity, *S*, of the $^5D_0 \rightarrow {}^7F_{0\text{-}4}$ transitions has been measured for compounds **1** at 300 K.

Because the $^5D_0 \rightarrow {}^7F_1$ transition does not depend on the local ligand field (due to its

dipolar magnetic nature) it may be used as a reference for the whole spectrum, *in vacuo* $A(^5D_0 \rightarrow {}^7F_1) = 14.65\ s^{-1}$,[6] and A_r is given by:

$$k_r = A_{0\rightarrow 1} \frac{\hbar\omega_{0\rightarrow 1}}{S_{0\rightarrow 1}} \sum_{J=0}^{4} \frac{S_{0-J}}{\hbar\omega_{0-J}} \qquad \text{(S5)}$$

where $A_{0\text{-}1}$ is the Einstein coefficient of spontaneous emission between the $^5D_0$ and the $^7F_1$ levels. An average index of refraction of 1.5 was considered for **1**, leading to $A(^5D_0 \rightarrow {}^7F_1) \approx 50\ s^{-1}$.[7]

REFERENCES

1. (a) D. Gatteschi, R. Sessoli and J. Villain, *Molecular Nanomagnets*, Oxford University, New York, 2006. (b) Y.-N. Guo, G.-F. Xu, P. Gamez, L. Zhao, S.-Y. Lin, R. Deng, J. Tang and H.-J. Zhang, *J. Am. Chem. Soc.*, 2010, 132, 8538-8539.
2. M. H. V. Werts, R. T. F. Jukes, J. W. Verhoeven, *Phys. Chem. Chem. Phys.*, 2002, 4, 1542-1548
3. L. D. Carlos, Y. Messaddeq, H. F. Brito, R. A. Sá Ferreira, V. De Zea Bermudez, S. J. L. Ribeiro, *Adv. Mater.*, 2000, 12, 594-598
4. O. L. Malta, H. F. Brito, J. F. S. Menezes, F. R. Gonçalves e Silva, S. Alves Jr., F. S. Farias Jr., A.V . M. Andrade, *J. Lumin.*, 1997, 75, 255-268
5. O. L. Malta, M. A. Couto dos Santos, L. C. Thompson, N. K. Ito, *J. Lumin.*, 1996, 69, 77-84.
6. M. F. Hazenkamp, G. Blasse, *Chem. Mater.*, 1990, 2, 105-110.
7. R. M. Supkowski, W. D. Horrocks, *Inorg. Chim. Acta*, 2002, 340, 44-48.

Table S1. Selected bond lengths (Å) and angles (°) for **1**-**5**

	1Eu·1.5CH_3OH	**2Tb**·0.5H_2O·CH_3OH	**3Dy**·H_2O	**4Ho**·0.5H_2O·CH_3OH	**5Er**·1.5H_2O
Ln1-O4	2.305(4)	2.287(3)	2.277(6)	2.266(3)	2.238(5)
Ln1-O3	2.360(4)	2.330(3)	2.319(6)	2.307(3)	2.288(5)
Ln1-O2	2.297(4)	2.261(3)	2.260(6)	2.260(3)	2.247(5)
Ln1-O1	2.313(4)	2.283(3)	2.272(6)	2.272(3)	2.260(5)
Ln1-N4	2.558(3)	2.523(4)	2.527(8)	2.518(4)	2.524(6)
Ln1-N3	2.554(3)	2.516(4)	2.508(8)	2.506(4)	2.470(6)
Ln1-N2	2.573(3)	2.530(4)	2.522(7)	2.524(4)	2.500(5)
Ln1-N1	2.554(3)	2.515(4)	2.522(7)	2.511(4)	2.478(6)
O4-Ln1-O3	151.69(10)	150.53(12)	150.0(2)	149.34(13)	148.66(19)
O2-Ln1-O1	151.13(10)	149.73(12)	148.9(2)	148.56(12)	148.29(17)
O1-Ln1-O3	101.97(13)	102.21(13)	101.9(2)	102.36(13)	102.82(19)
O2-Ln1-O4	97.81(13)	98.65(13)	98.1(2)	98.49(13)	98.79(19)
O2-Ln1-O3	87.72(13)	87.61(13)	88.1(2)	88.21(12)	87.82(18)
O1-Ln1-O4	86.50(13)	86.80(14)	87.8(2)	87.41(14)	87.5(2)
O4-Ln1-N1	80.97(11)	80.49(13)	80.4(3)	80.18(13)	79.74(19)
O1-Ln1-N3	80.46(12)	79.78(13)	79.0(2)	79.18(13)	79.09(18)
O2-Ln1-N4	80.92(12)	79.86(13)	79.2(2)	78.91(13)	79.02(18)
O3-Ln1-N2	79.70(12)	79.00(12)	78.9(2)	78.70(12)	78.20(18)
O2-Ln1-N3	77.29(12)	76.62(12)	76.5(2)	76.41(12)	76.19(17)
O3-Ln1-N1	76.60(12)	76.06(12)	76.0(2)	75.62(12)	75.66(17)
O4-Ln1-N2	75.97(12)	75.83(13)	75.3(2)	75.12(13)	74.85(19)
O1-Ln1-N4	73.54(12)	73.76(13)	73.8(3)	73.68(13)	73.54(19)
O2-Ln1-N2	71.17(11)	71.61(12)	71.9(2)	71.98(12)	72.22(17)
O1-Ln1-N1	70.80(11)	71.59(13)	71.8(2)	71.78(13)	72.08(18)
O4-Ln1-N4	70.90(11)	71.23(13)	71.5(3)	71.77(14)	71.7(2)
O3-Ln1-N3	70.47(10)	70.65(13)	71.0(2)	71.17(12)	71.40(18)
O2-Ln1-N1	138.06(11)	138.63(12)	139.3(2)	139.61(13)	139.58(18)
O4-Ln1-N3	137.84(10)	138.81(13)	139.0(3)	139.49(14)	139.9(2)
O1-Ln1-N2	137.02(11)	138.08(12)	138.7(2)	138.83(13)	138.89(18)

Table S2. The CSM and Δ values for complexes **1** – **5**.

CSM and Δ	**1Eu**·1.5CH_3OH	**2Tb**·0.5H_2O·CH_3OH	**3Dy**·H_2O	**4Ho**·0.5H_2O·CH_3OH	**5Er**·1.5H_2O
square antiprism D_{4d}	2.41022	2.20235	2.22767	2.13430	2.07817
dodecahedron D_{2d}	1.26125	1.11645	1.04025	1.01486	0.98597
Δ	0.58295	0.50269	0.48601	0.45973	0.43965

Table S3. Hydrogen bonds of **1Eu**·1.5CH_3OH

D-H···A	*d* (D-H) / Å	*d* (H-A) / Å	*d* (D-A) / Å	∠ (D-H-A) / °
N9-H9C···O13	0.90	1.86	2.729(6)	162
O13-H13B···O3	0.84	2.03	2.830(6)	159
C8-H8B···O10	0.99	2.45	3.428(7)	171
C9-H9B···O11	0.99	2.54	3.481(7)	159
C24-H24B···O5	0.99	2.38	3.310(8)	157
C19-H19A···O14i	0.95	2.33	3.265(13)	169
C29-H29A···O8ii	0.95	2.53	3.467(8)	171
C21-H21A···O7iii	0.95	2.59	3.414(5)	145
C23-H23A···O7iii	0.95	2.60	3.458(5)	150
C7-H7A···O12iv	0.95	2.66	3.461(9)	142

Symmetry codes: i: 1-x, 1-y, -z; ii: -x, 2-y, 1-z; iii: 1-x, 1-y, 1-z; iv: -x, 2-y, -z.

Table S4. Hydrogen bonds of **2Tb**·0.5H_2O·CH_3OH

D-H···A	*d* (D-H) / Å	*d* (H-A) / Å	*d* (D-A) / Å	∠ (D-H-A) / °
C8-H8B···O9’	0.97	2.33	3.318 (3)	146
C10-H10···O9’i	0.93	2.50	3.340 (2)	165
C8-H8B···O10	0.97	2.46	3.426(8)	173
C9-H9B···O11	0.97	2.55	3.478(10)	159
C9-H9B···O11’	0.93	2.51	3.340 (2)	153
C24-H24B···O5	0.97	2.36	3.299(11)	162
N9-H9C···O13	0.91	1.87	2.747(7)	160
O13-H13A···O3	0.82	2.08	2.870(7)	161

Symmetry code: i: 1-x, 2-y, -z. O9’ occupancy 0.135(7); O11’ occupancy 0.232(7)

Table S5. Hydrogen bonds of **3Dy**·H_2O

D-H···A	*d* (D-H) / Å	*d* (H-A) / Å	*d* (D-A) / Å	∠ (D-H-A) / °
C8-H8B···O9’	0.97	2.50	3.332(57)	144
C10-H10···O9’i	0.93	2.40	3.31(4)	166
C8-H8B···O10	0.97	2.42	3.392(17)	175
C9-H9B···O11	0.97	2.53	3.45(2)	158
C9-H9B···O11’	0.97	2.56	3.46(4)	153
C24-H24B···O5	0.97	2.34	3.28(2)	162
N9-H9C···O1W	0.91	1.86	2.734(18)	157
C24-H24B···O6’ii	0.97	2.49	3.08(3)	119
C21-H21···O7iii	0.93	2.67	3.49(1)	148
C23-H23···O7iii	0.93	2.71	3.56(1)	152
C29-H29···O8iv	0.93	2.57	3.492(18)	170

Symmetry codes: i: 1-x, 2-y, -z; ii: -x, 1-y, 1-z; iii: 1-x, 1-y, 1-z; iv: -x, 2-y, -z;. O9’ occupancy 0.137(12); O11’ occupancy 0.265(14); O6’ occupancy 0.398(17).

Table S6. Hydrogen bonds of **4Ho**·0.5H_2O·CH_3OH

D-H···A	*d* (D-H) / Å	*d* (H-A) / Å	*d* (D-A) / Å	∠ (D-H-A) / °
C8-H8B···O9’	0.97	2.38	3.32(3)	144
C10-H10···O9’i	0.93	2.44	3.35(2)	166
C8-H8B···O10	0.97	2.42	3.390(10)	174
C9-H9B···O11	0.97	2.54	3.459(10)	159
C9-H9B···O11’	0.97	2.51	3.40(2)	152
C24-H24B···O5	0.97	2.35	3.292(12)	164
N9-H9C···O13	0.91	1.91	2.777(8)	158
O13-H13A···O3	0.82	2.12	2.904(8)	161

Symmetry code: i: 1-x, 2-y, -z. O9’ occupancy 0.151(8); O11’ occupancy 0.230(7)

Table S7. Hydrogen bonds of **5Er**·1.5H_2O

D-H···A	*d* (D-H) / Å	*d* (H-A) / Å	*d* (D-A) / Å	∠ (D-H-A) / °
C8-H8B···O9’	0.97	2.49	3.32(4)	143
C10-H10···O9’i	0.93	2.31	3.22(2)	166
C8-H8B···O10	0.97	2.41	3.374(13)	174
C9-H9B···O11	0.97	2.49	3.413(16)	159
C9-H9B···O11’	0.97	2.54	3.43(3)	152
C24-H24B···O5	0.97	2.32	3.261(17)	163
N9-H9C···O1W	0.91	1.88	2.734(13)	156

Symmetry code: i: 1-x, 2-y, -z. O9’ occupancy 0.150(9); O11’ occupancy 0.243(11)

Table S8. The parameters obtained by fitting the *ac* magnetic susceptibilities of compound **3Dy**·H_2O at 2.0 K in indicated *dc* fields.

H / kOe	χ_T / $cm^3 \cdot mol^{-1}$	χ_S / $cm^3 \cdot mol^{-1}$	ln(τ/ s)	α	R^a
0	5.65	0.00	-11.16	0.01	7.0×10^{-6}
0.5	5.59	1.39	-6.86	0.34	1.4×10^{-4}
1.0	5.27	0.43	-4.99	0.46	2.8×10^{-4}
1.5	4.84	0.25	-3.98	0.51	3.8×10^{-4}
2.0	4.12	0.20	-3.58	0.52	8.8×10^{-4}
2.5	3.60	0.18	-3.32	0.53	1.8×10^{-3}
3.0	2.75	0.22	-3.58	0.48	2.8×10^{-4}

[a] $R = \sum\left[(\chi'_{obs}-\chi'_{cal})^2 + (\chi''_{obs}-\chi''_{cal})^2\right] / \sum\left[\chi'^2_{obs} + \chi''^2_{obs}\right]$

Table S9. The parameters obtained by fitting the *ac* magnetic susceptibilities of compound **3Dy**·H_2O under 1.5 kOe *dc* field.

T / K	χ_T / $cm^3 \cdot mol^{-1}$	χ_S / $cm^3 \cdot mol^{-1}$	ln(τ / s)	α	R[a]
1.8	6.75	0.24	-3.83	0.54	2.9×10^{-5}
2	6.44	0.27	-3.74	0.54	3.7×10^{-5}
3	4.66	0.43	-3.99	0.48	1.7×10^{-4}
4	3.46	0.52	-4.64	0.39	3.8×10^{-4}
5	2.73	0.54	-5.39	0.30	4.5×10^{-4}
6	2.26	0.54	-6.14	0.24	3.2×10^{-4}
7	1.94	0.54	-6.82	0.21	2.4×10^{-4}
8	1.70	0.56	-7.45	0.20	1.6×10^{-4}
9	1.51	0.60	-8.01	0.19	1.1×10^{-4}
10	1.36	0.64	-8.53	0.19	6.6×10^{-5}

[a] $R = \sum\left[(\chi'_{obs}-\chi'_{cal})^2 + (\chi''_{obs}-\chi''_{cal})^2\right] / \sum\left[\chi'^{2}_{obs} + \chi''^{2}_{obs}\right]$

Table S10. The parameters obtained by fitting the *ac* magnetic susceptibilities of compound **5Er**·1.5H_2O under 1.5 kOe *dc* field.

T / K	χ_T / $cm^3 \cdot mol^{-1}$	χ_S / $cm^3 \cdot mol^{-1}$	ln(τ / s)	α	R
1.8	2.38	0.60	-8.73	0.21	1.1×10^{-4}
1.9	2.31	0.02	-9.32	0.26	5.7×10^{-5}
2	2.23	0.05	-9.40	0.24	4.5×10^{-5}
2.1	2.16	0.08	-9.47	0.23	2.4×10^{-5}
2.2	2.09	0.27	-9.39	0.20	3.4×10^{-5}
2.3	2.02	0.08	-9.67	0.22	3.1×10^{-5}
2.4	1.96	0.19	-9.68	0.20	2.5×10^{-5}
2.6	1.84	0.03	-10.04	0.18	1.6×10^{-5}
2.8	1.74	0.03	-10.25	0.16	1.8×10^{-5}
3.0	1.64	0.03	-10.48	0.13	2.3×10^{-5}

Table S11. The parameters obtained by fitting the *ac* magnetic susceptibilities of compound **6Yb** in indicated *dc* field at 2 K.

H / kOe	χ_T / $cm^3 \cdot mol^{-1}$	χ_S / $cm^3 \cdot mol^{-1}$	ln(τ / s)	α	R
0.5	0.40	0.20	-8.57	0.07	1.2×10^{-5}
1.0	0.40	0.14	-8.63	0.08	2.9×10^{-5}
1.5	0.39	0.12	-8.64	0.09	6.3×10^{-5}
2.0	0.39	0.10	-8.68	0.11	3.3×10^{-5}
2.5	0.38	0.09	-8.69	0.13	1.4×10^{-4}
3.0	0.37	0.08	-8.75	0.18	1.3×10^{-3}

Table S12. The parameters obtained by fitting the *ac* magnetic susceptibilities of compound **6Yb** under 1.5 kOe *dc* field.

T / K	χ_T / cm^3·mol^{-1}	χ_S / cm^3·mol^{-1}	ln(τ/ s)	α	R
2.0	0.39	0.12	-8.64	0.09	6.3×10^{-5}
2.2	0.36	0.14	-8.95	0.07	5.2×10^{-5}
2.4	0.33	0.15	-9.26	0.08	5.2×10^{-5}
2.6	0.31	0.16	-9.60	0.09	6.3×10^{-5}
2.8	0.28	0.19	-9.65	0.06	3.1×10^{-5}

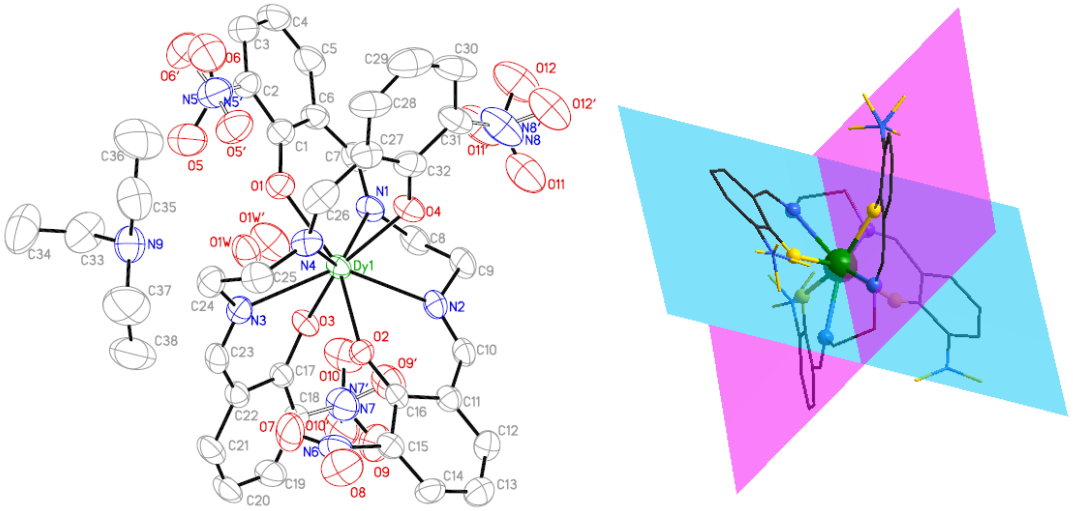

Figure S1. Left: The molecular structure of **3Dy**·H_2O (50% probability); Right: The mononuclear structure of [Dy(3-NO_2salen)$_2$]$^-$ with two perpendicular ligands.

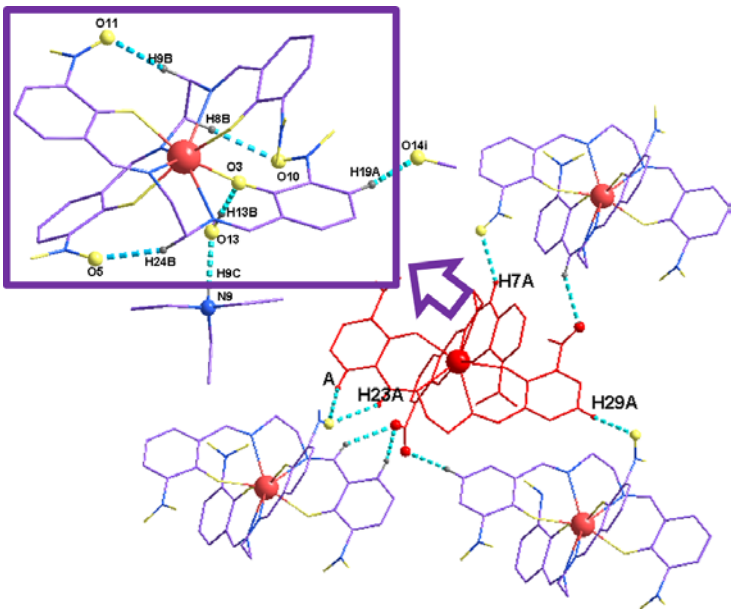

Figure S2. The intra- and inter hydrogen bond interactions in structure **1Eu**·1.5CH_3OH. H atoms are omitted for clarity except for those involved in hydrogen bonds. Symmetry code: i: 1-x, 1-y, -z

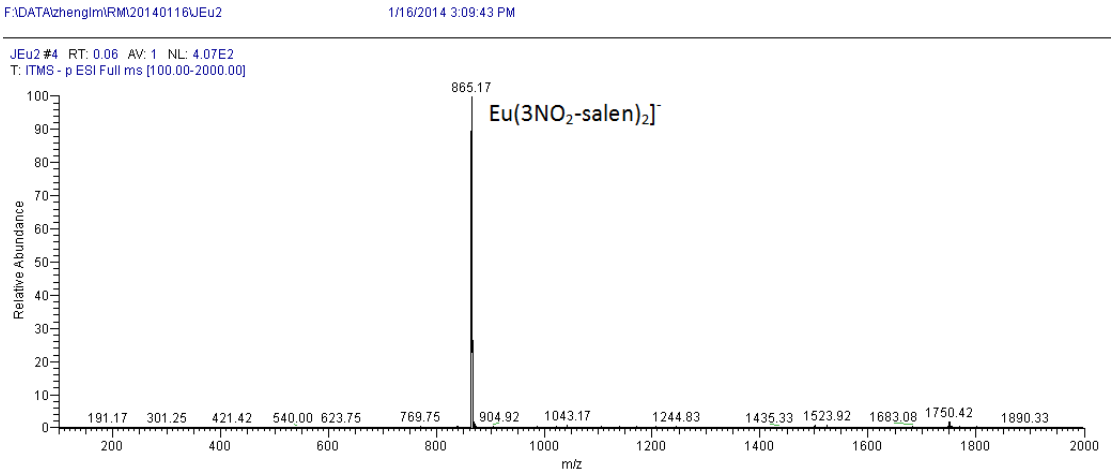

Figure S3. Negative ion electrospray ionization mass spectrum of **1Eu**

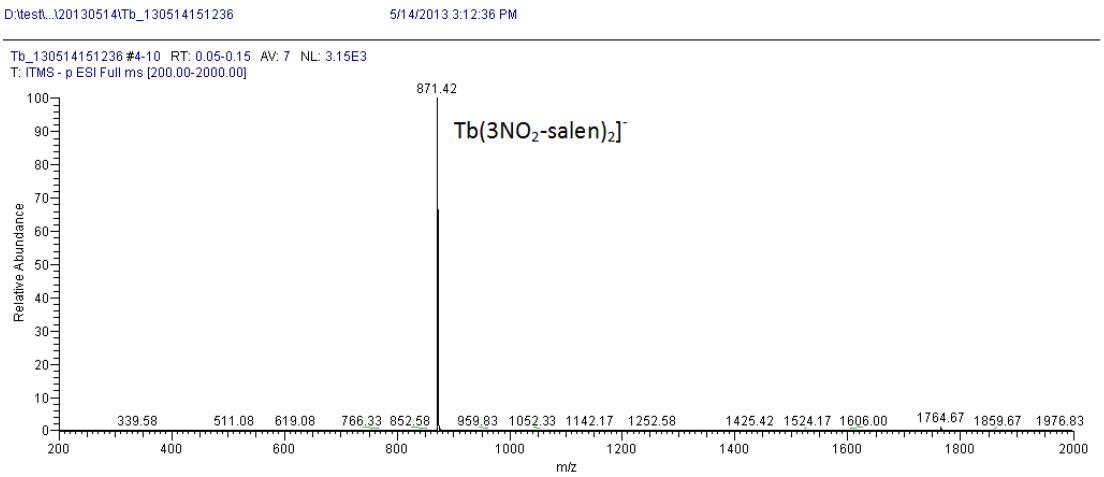

Figure S4. Negative ion electrospray ionization mass spectrum of **2Tb**

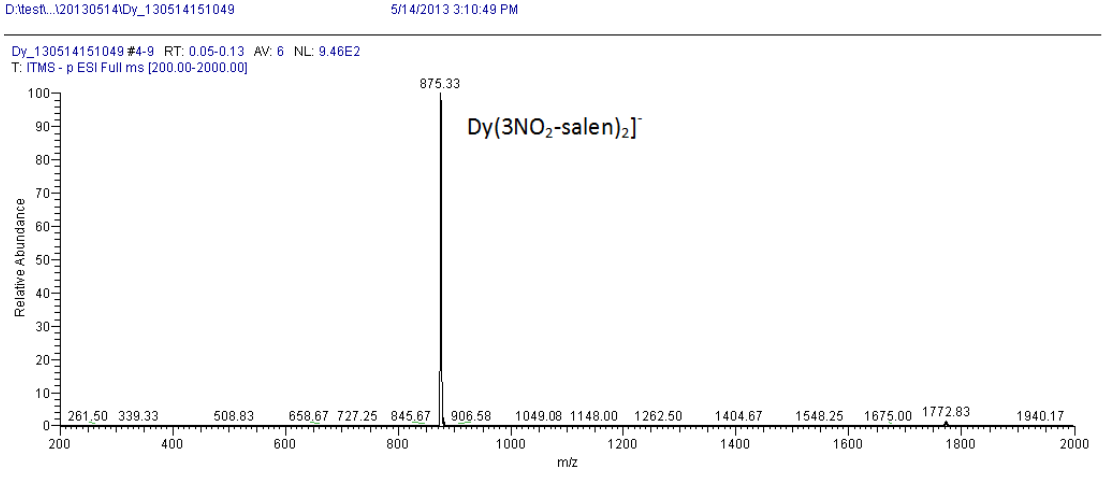

Figure S5. Negative ion electrospray ionization mass spectrum of **3Dy**

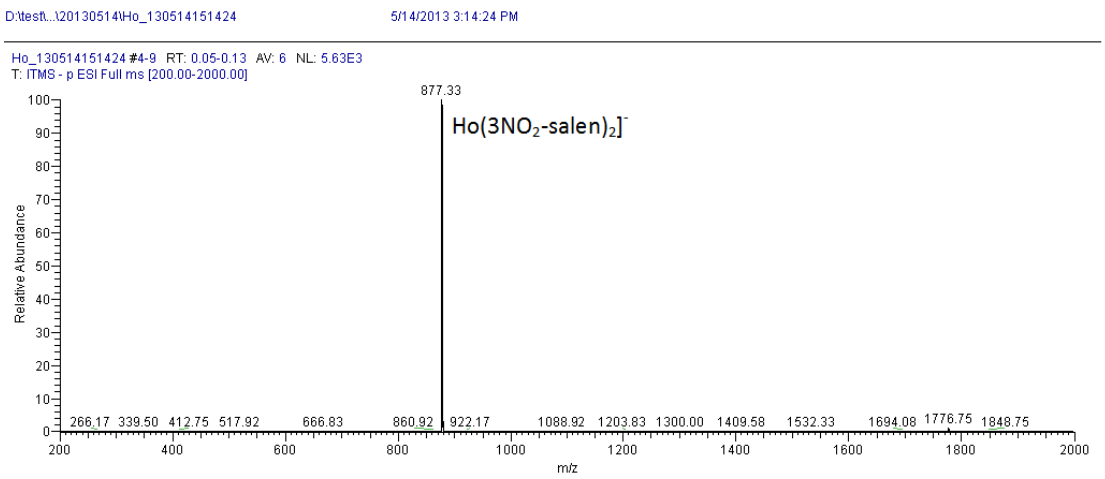

Figure S6. Negative ion electrospray ionization mass spectrum of **4Ho**

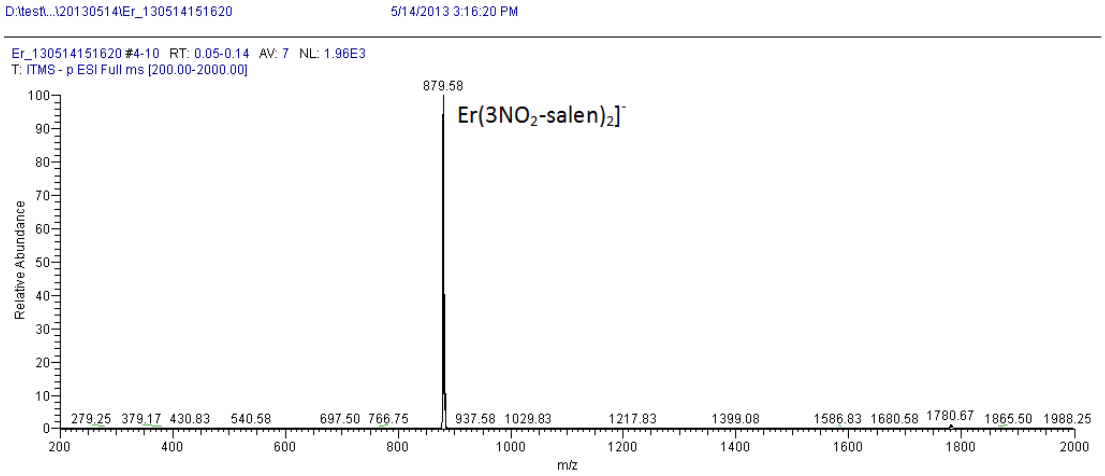

Figure S7. Negative ion electrospray ionization mass spectrum of **5Er**

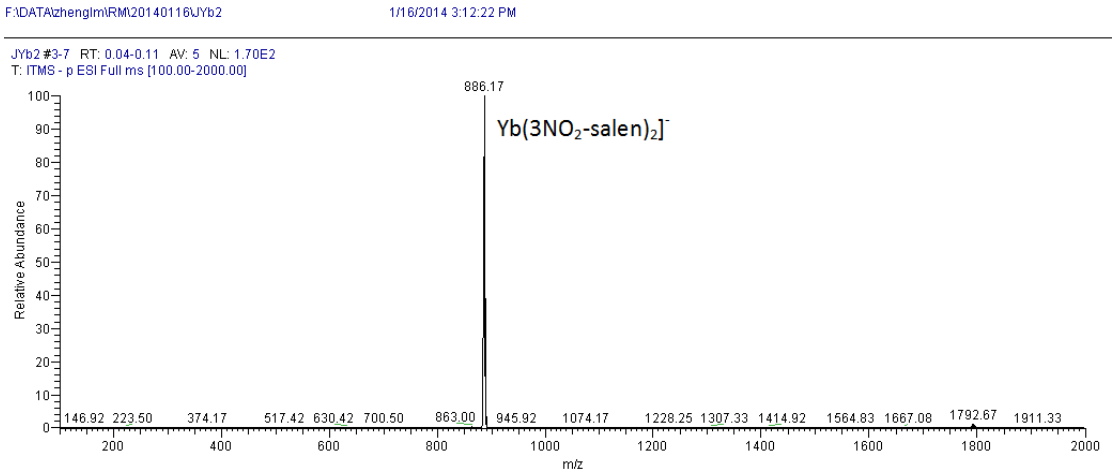

Figure S8. Negative ion electrospray ionization mass spectrum of **6Yb**

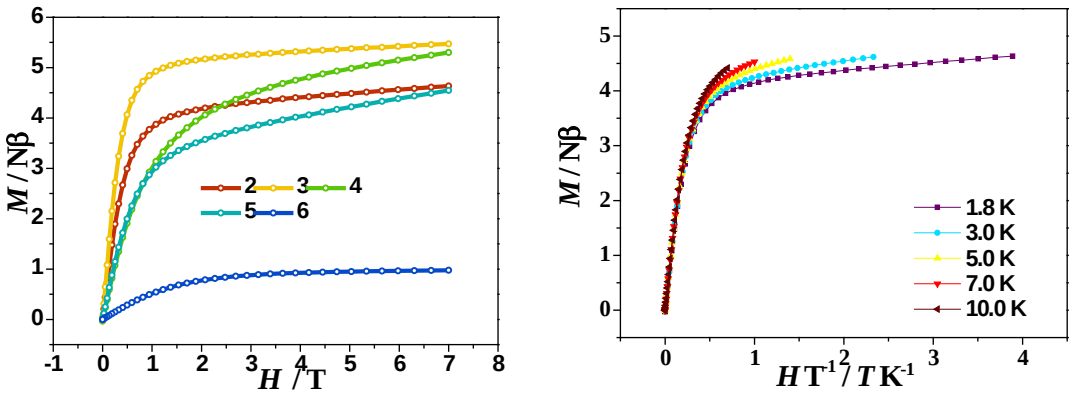

Figure S9. The *M* vs. *H* plots at 1.8 K for **2** -**6** (left) and the *M* vs. *H*/*T* plots of **2Tb**·0.5H_2O·CH_3OH (right) at indicated temperatures.

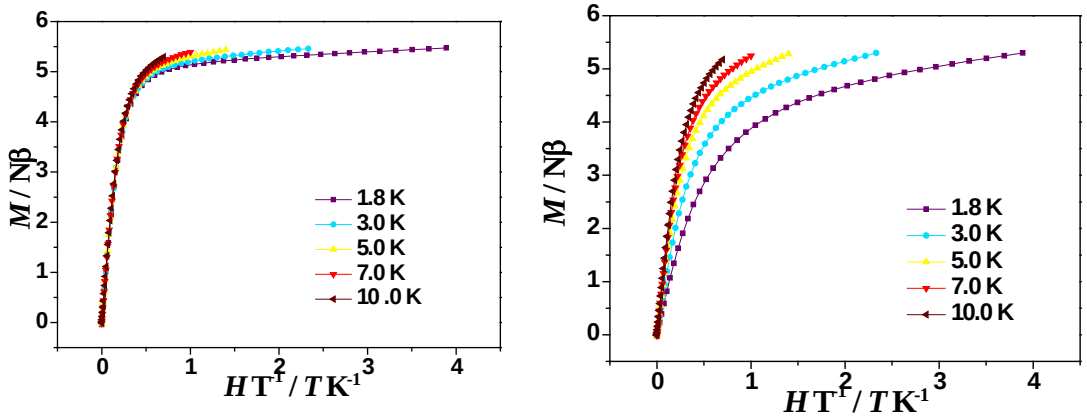

Figure S10. The *M* vs. *H*/*T* plots of **3Dy**·H_2O (left) and **4Ho**·0.5H_2O·CH_3OH (right) at indicated temperatures.

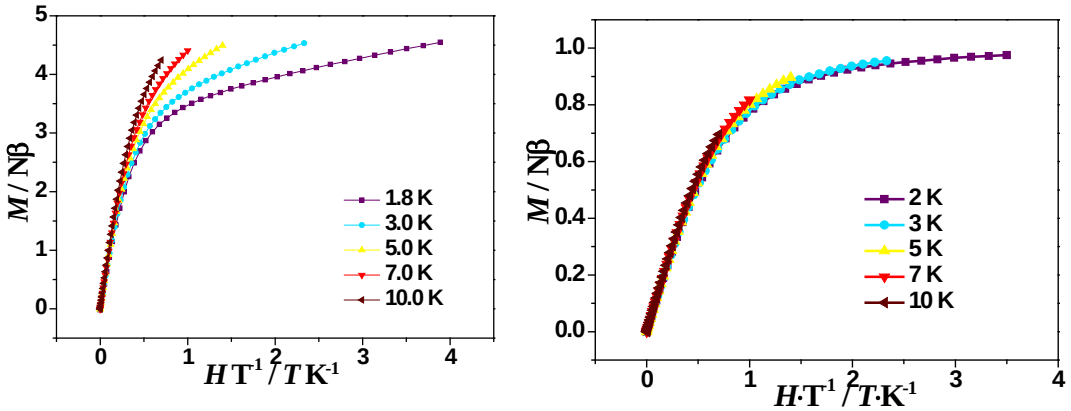

Figure S11. The *M* vs. *H*/*T* plots of **5Er**·1.5H_2O (left) and **6Yb** (right) at indicated temperatures.

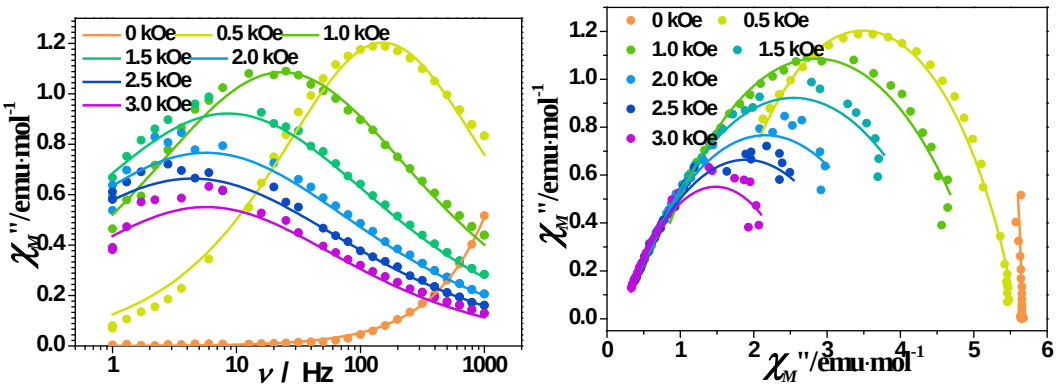

Figure S12. Variable-frequency out-of-phase ac susceptibility data (left) and Cole-Cole plots of **3Dy**·H_2O at 2 K under indicated external dc fields. The solid lines represent the best fits according to Debye model.

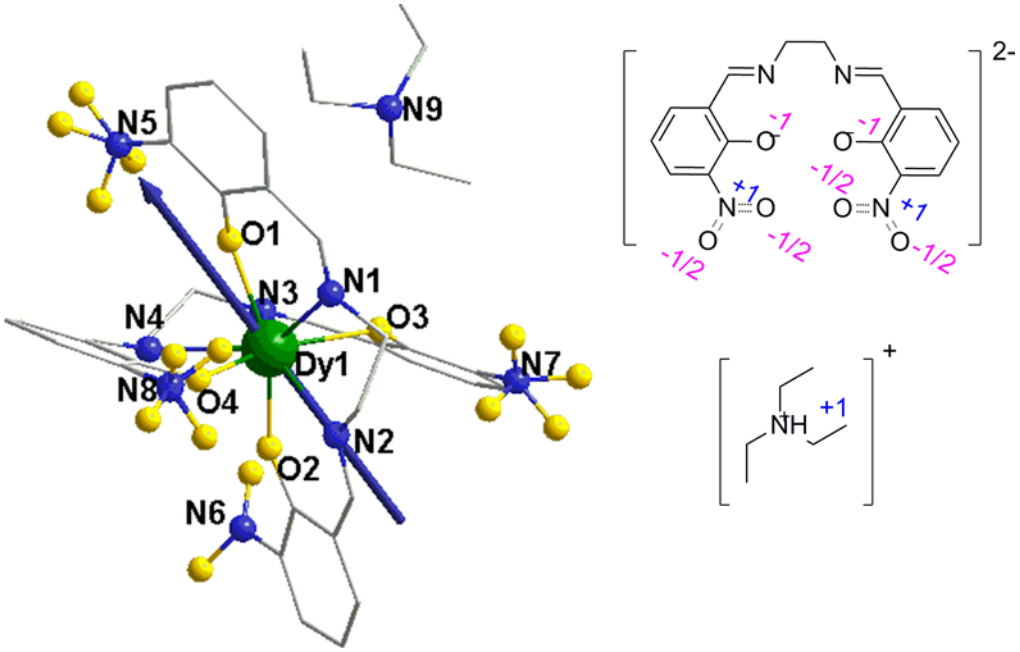

Figure S13. The orientation of the magnetic anisotropy is estimated by using MAGELLAN software. The mononuclear $[Dy(3\text{-}NO_2salen)_2]^-$ and $(Et_3N)^+$ counterion are considered in the calculation. Left: The calculated easy-axis (blue arrow) in **3Dy**·H_2O. Right: The partial charges of the $3\text{-}NO_2salen^{2-}$ ligand and $(Et_3N)^+$. The direction of the arrow head is arbitrary.

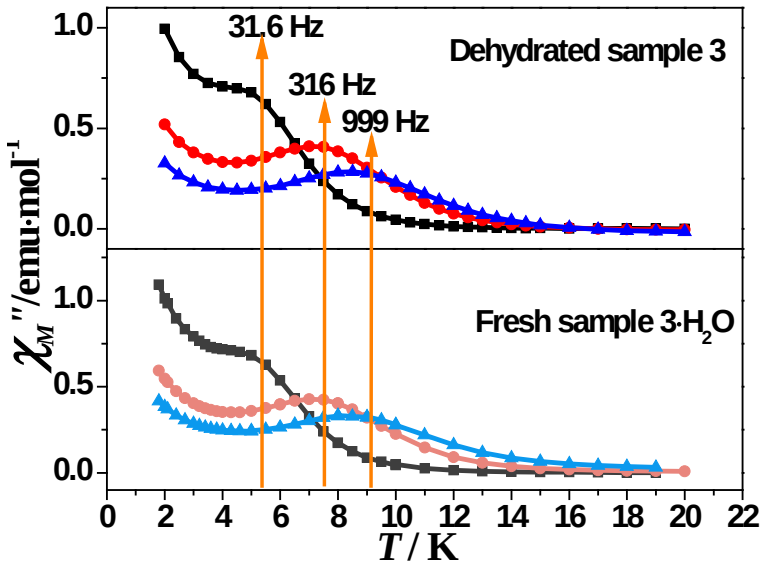

Figure S14. Variable-temperature out-of-phase ac susceptibility data of fresh sample **3Dy**·H_2O and dehydrated sample of **3Dy** from 2 to 20 K at indicated frequencies.

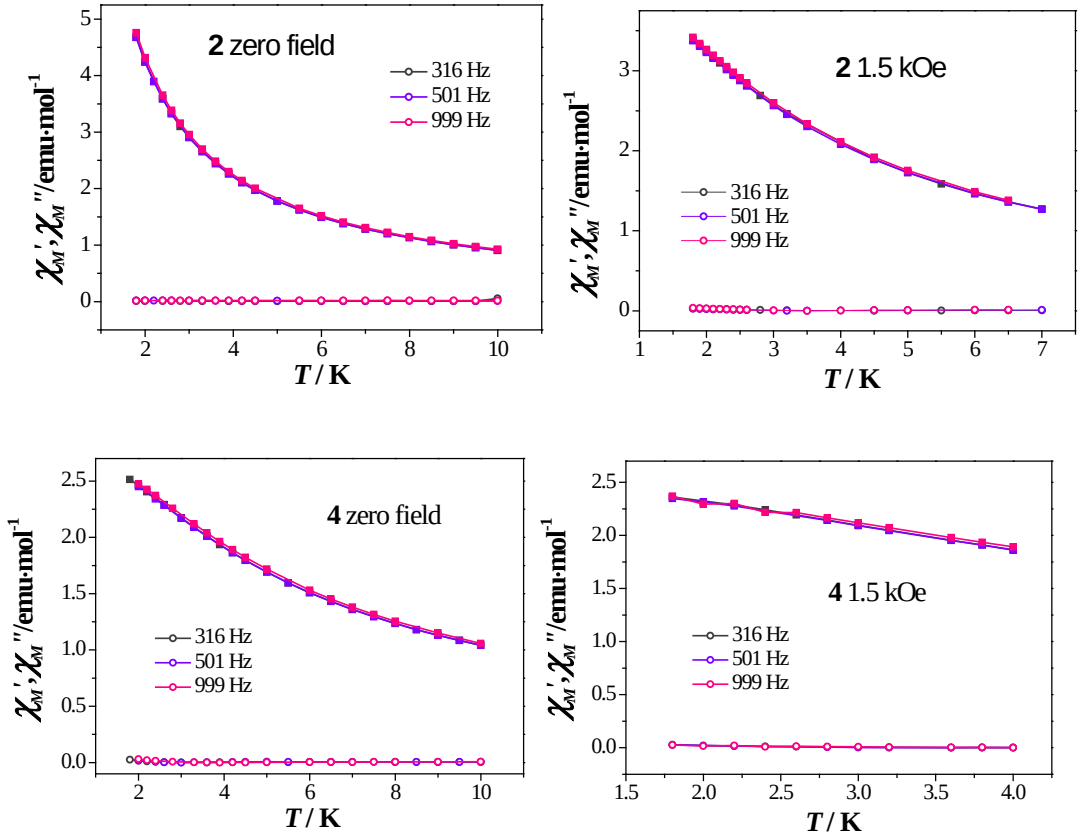

Figure S15. Variable-temperature ac susceptibility data of **2Tb**·0.5H_2O·CH_3OH (up) and **4Ho**·0.5H_2O·CH_3OH (down) in zero static field (left) and 1.5 kOe dc field (right). The square represents the in-phase ac magnetic susceptibility, and the circle represents out-of-phase ac magnetic susceptibility.

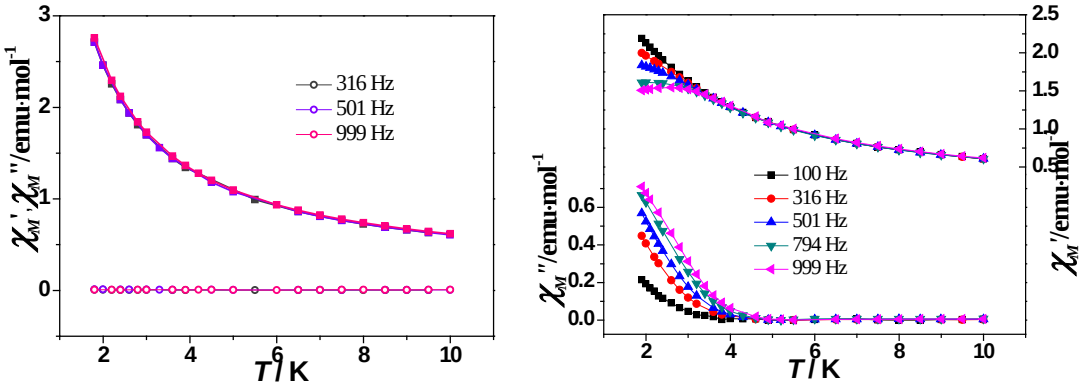

Figure S16. Variable-temperature ac susceptibility data of **5Er**·1.5H_2O in zero static field (left) and 1.5 kOe dc field (right).

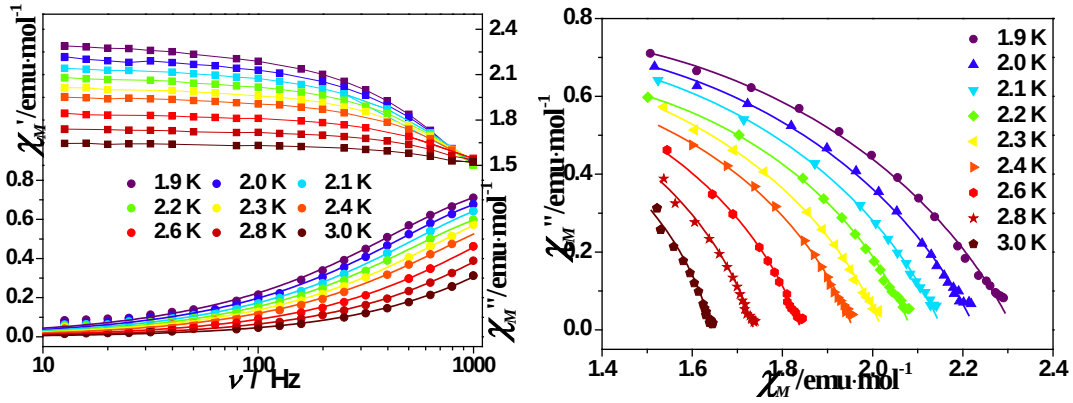

Figure S17. Variable- frequency ac susceptibility data (left) and Cole-Cole plots (right) of **5Er**·1.5H_2O in 1.5 kOe dc field. The solid line represents the best fits according to Arrhenius law.

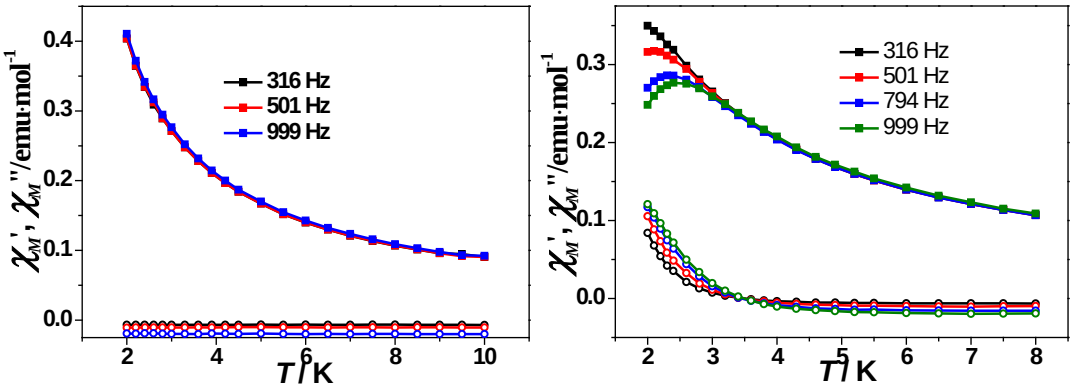

Figure S18. Variable-temperature ac susceptibility data of **6Yb** in zero static field (left) and 1.5 kOe dc field (right).

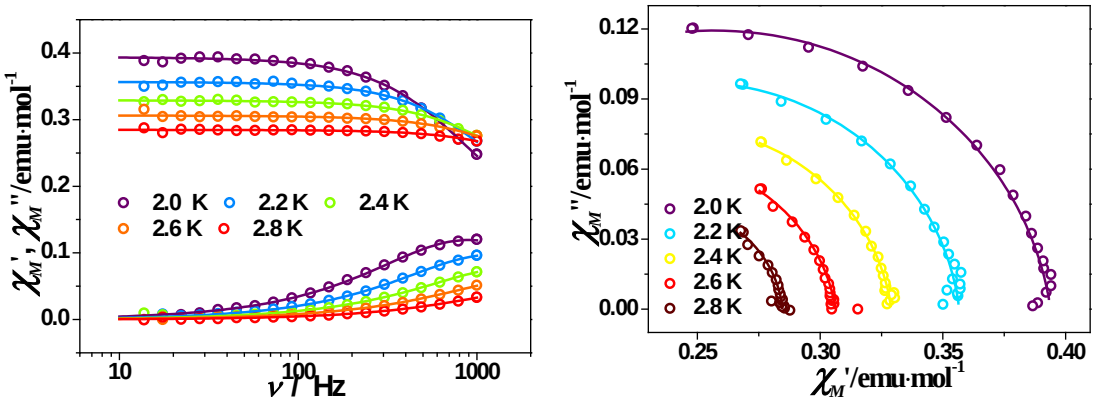

Figure S19. Variable- frequency ac susceptibility data (left) and Cole-Cole plots (right) of **6Yb** in 1.5 kOe dc field. The solid line represents the best fits according to Arrhenius law.

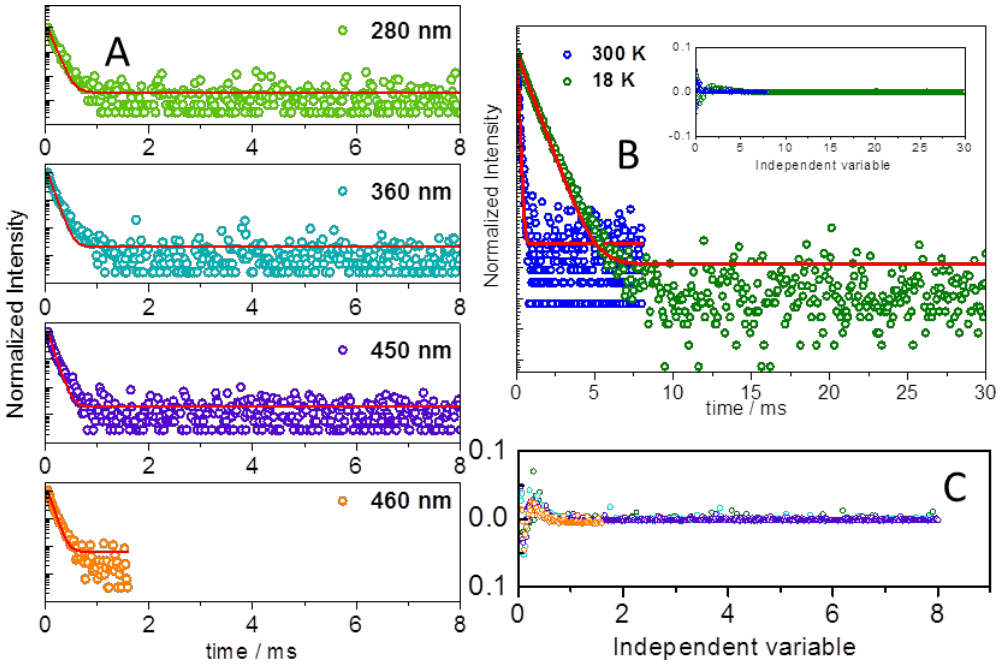

Figure S20. Emission decay curves of **1Eu** (A) excited at 280 nm, 360nm, 450 nm and 460 nm and monitored at 612 nm and (B) excited at 460 nm and acquired at 18 K and 300 K. The solid lines represented the best fit using a single exponential function (R>0.994). The fit residual plots are also shown at the bottom (C).

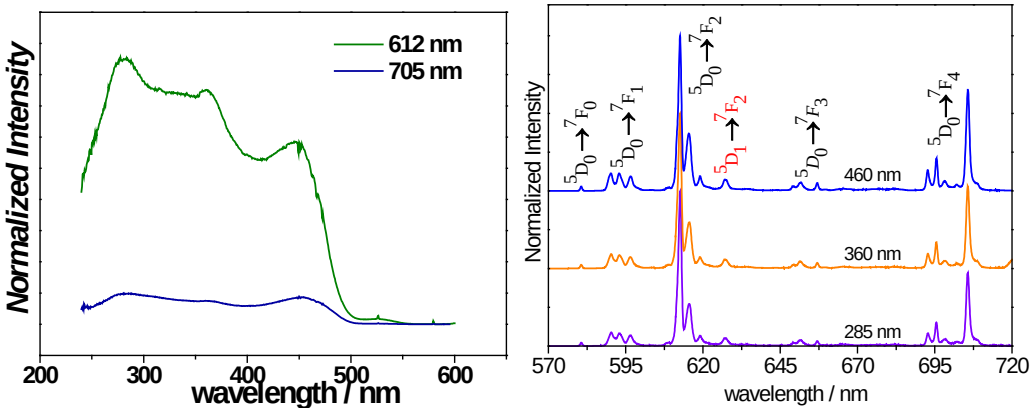

Figure S21. The excitation (left) and emission (right) spectra of **1Eu** recorded at 14 K.

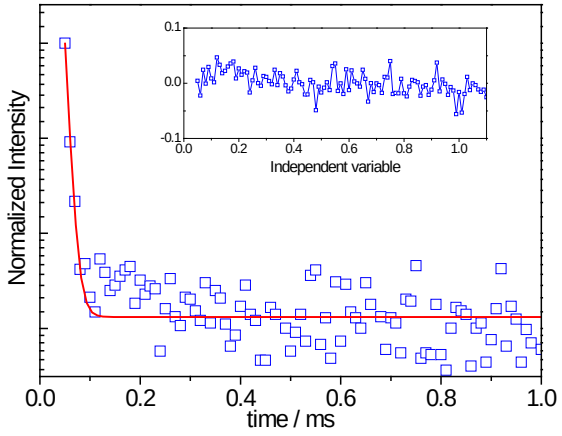

Figure S22. Room temperature emission decay curves of **6Yb** excited at 460 nm and monitored at 995 nm. The solid line represents the best fit using a single exponential function (R>0.98). The fit residual plot is also shown (inset).